

Cite this: *J. Mater. Chem. C*, 2017,
5, 11910

Simultaneously tuning the emission color and improving thermal stability *via* energy transfer in apatite-type phosphors

Dan Wu,^{ab} Wenge Xiao,^{ab} Liangliang Zhang,^{*a} Xia Zhang,^a Zhendong Hao,^a Guo-Hui Pan,^a Yongshi Luo^a and Jiahua Zhang^{*a}

Developing phosphors with high quantum efficiency and superior thermal stability is still a challenge for phosphor-converted white light-emitting diodes (w-LEDs). Energy transfer between ions is usually utilized to tune the emission wavelength. In this study, we demonstrate that in addition to the tunable emission color, an improved thermal stability can be achieved by energy transfer from Ce³⁺ to Tb³⁺ in Ce³⁺ and Tb³⁺ codoped Ba₂Y₃(SiO₄)₃F (BYSF:Ce³⁺,Tb³⁺) phosphors without quantum efficiency loss, which is ascribed to the combined effect of fast energy transfer within the nearest Ce³⁺–Tb³⁺ pairs *via* electric dipole–quadrupole interactions, and the following energy diffusion among the Tb³⁺ ions. An efficient energy transfer from Ce³⁺ to Tb³⁺ results in the novel green phosphor BYSF:2%Ce³⁺,40%Tb³⁺ with an internal quantum efficiency of as high as 83.12%. In addition, a w-LED lamp was fabricated to explore its possible application in w-LEDs based on near UV LEDs. Our results indicate that fast energy transfer to Tb³⁺ may provide an alternative way of improving the thermal stability of phosphors.

Received 29th August 2017,
Accepted 30th October 2017

DOI: 10.1039/c7tc03941g

rsc.li/materials-c

1. Introduction

To address the challenges of energy conservation and environmental protection issues, white light-emitting diodes (w-LEDs), possessing the advantages of long lifetimes, high brightness, robustness, and environmental friendliness, are undergoing rapid development and have been considered as the next-generation of lighting technology.^{1–3} At present, the most common way to generate white light is combining a blue InGaN LED chip with the well-known yellow phosphor Y₃Al₅O₁₂:Ce³⁺ (YAG:Ce³⁺). However, the application of w-LEDs faces the problem of lacking a sufficient cyan or red component in emission, thus requiring additional phosphors.^{4–6} An alternative way of solving this problem is the fabrication of w-LEDs by using near ultraviolet (n-UV) LED chips (350–420 nm) and tricolor (red, green, and blue) phosphors, which is expected to generate white light with a high color rendering index (CRI) and a low correlated color temperature (CCT).^{6–8} Undoubtedly, the luminescence properties of tricolor phosphors determine the eventual performance of w-LEDs, and hence it is of great significance to find new phosphors with high

quantum efficiencies (QEs) and good thermal stability that can be excited by n-UV LEDs.

Rare earth (RE) Ce³⁺ is a commonly used efficient active ion in phosphors for w-LEDs due to the parity-allowed 4f–5d transition. The emission color of the Ce³⁺ 5d–4f transition varies from ultraviolet to blue and even to red according to the local environment since the 5d orbital strongly interacts with its surroundings.^{9–11} However, the broad emission band originating from 5d–4f transition of singly activated phosphors still cannot cover the whole visible spectral range to generate ideal white light. Additionally, though many Ce³⁺ activated phosphors have high QEs, they cannot yet be applied for w-LEDs because their emission is shorter than 440 nm, which is negligible for white light and even harmful to human eyes.^{9,12} Hence, it is important to tune the emission, by enriching the cyan or red component or fully converting those short wavelengths (<440 nm) to longer ones in emission. This can be realized by two common strategies, one is formation of solid solution phosphors by cation or anion substitution,^{11,13,14} the other is codoping another activator that emits longer wavelength light such as RE ions Eu²⁺, Pr³⁺ and Tb³⁺ and transition metal ions Mn²⁺ and Cr³⁺, thereby regulating the emission color of the phosphors by an energy transfer process.^{15,16} The latter has been intensively studied, such as in Ce³⁺/Mn²⁺,^{17,18} Ce³⁺/Pr³⁺,^{19,20} Ce³⁺/Eu²⁺,^{21,22} and Ce³⁺/Cr³⁺,²³ since multi-emission peaks or even white light can be achieved in a single host crystal.

^a State Key Laboratory of Luminescence and Applications, Changchun Institute of Optics, Fine Mechanics and Physics, Chinese Academy of Sciences, 3888 Eastern South Lake Road, Changchun 130033, China. E-mail: zhangliangliang@ciomp.ac.cn, zhangjh@ciomp.ac.cn

^b University of Chinese Academy of Sciences, Beijing, 100049, China

On the other hand, thermal stability is a key parameter for phosphors.^{24–26} Since the transitions of f–d (Ce^{3+} or Eu^{2+}) and d–d (Mn^{2+} and Cr^{3+}) are sensitive to the crystal environment, the thermal stability of their emissions strongly depends on the structural and optical properties of the host crystals, most of which show limited thermal stability. As for Pr^{3+} and Eu^{3+} , the overall QE will be largely lowered when they are used as acceptors because the related 4f levels of Pr^{3+} suffer strong multi-phonon relaxation and there exists metal–metal charge transfer quenching between Eu^{3+} and Ce^{3+} .^{19,20,27,28} Another important RE ion, Tb^{3+} , is well known for its intense green emission even in metal–organic compounds whose cutoff phonon energy is relatively large.^{29,30} Its predominant emission peak is around 545 nm originating from the $^5\text{D}_4 \rightarrow ^7\text{F}_5$ transition. However, the excitation band due to $4f^6-4f^75d^1$ parity-allowed transitions is located in the deep UV region (< 300 nm), which is beyond the emission of the available n-UV LED chips. Sensitizer like Ce^{3+} is needed to obtain efficient green phosphors for w-LEDs based on n-UV LEDs. As we know, Tb^{3+} has a unique and attractive energy level structure whereby the $^5\text{D}_4$ level is about $15\,000\text{ cm}^{-1}$ away from its next lowest level, rendering the multi-phonon relaxation negligible.^{31,32} Hence, the emission of the $^5\text{D}_4$ level usually has high QE and superior thermal stability. Besides, the $^5\text{D}_4$ level undergoes slow concentration quenching permitting a high doping level, which is beneficial to enhance the energy transfer efficiency from the sensitizer to Tb^{3+} . Recently, codoping with Tb^{3+} has been used to tune the emission color of Ce^{3+} (or Eu^{2+}) activated phosphors, such as $\text{CaScAlSiO}_6:\text{Ce}^{3+},\text{Tb}^{3+}$,¹⁸ $\text{CeF}_3:\text{Tb}^{3+}/\text{LaF}_3$,³³ $\text{NaBaScSi}_2\text{O}_7:\text{Ce}^{3+},\text{Tb}^{3+}$,³⁴ and $\text{Sr}_3\text{CaBa}(\text{PO}_4)_3\text{Cl}:\text{Eu}^{2+},\text{Tb}^{3+}$,³⁵ where the emission color can be largely tuned from violet/blue to green as the content of Tb^{3+} is increased. In our previous work, we have demonstrated that if the energy transfer rate from Ce^{3+} to Tb^{3+} is large enough to compete with the thermal quenching rate of its 5d emission, the excitation energy of the Ce^{3+} 5d level will be captured by the thermally stable Tb^{3+} $^5\text{D}_4$ level before thermal quenching happens, thereby improving the overall thermal stability.³⁶ Considering the above characteristics, codoping Tb^{3+} is expected to be utilized to tune the emission color and improve the thermal stability simultaneously.

Ce^{3+} doped apatite oxyfluoride $\text{Ba}_2\text{Y}_3(\text{SiO}_4)_3\text{F}$ (BYSF: Ce^{3+}) was reported to be a bluish violet phosphor that peaks at 425 nm with very high QE, but has poor thermal stability, thus it is useless for applications.³⁷ Herein, we introduced Tb^{3+} into BYSF: Ce^{3+} and thus obtained a highly efficient green phosphor with improved thermal stability as well as without a reduction in QE. The efficient energy transfer from Ce^{3+} to Tb^{3+} , the improved thermal stability as well as the potential application for w-LEDs were investigated in detail.

2. Experimental

2.1. Sample preparation

The powder samples were synthesized by the high-temperature solid-state reaction with the raw materials of high-purity, BaCO_3 , BaF_2 , Y_2O_3 , SiO_2 , CeO_2 , and Tb_4O_7 . They were weighed

stoichiometrically according to the composition of BYSF: $2\%\text{Ce}^{3+}, x\%\text{Tb}^{3+}$. After thorough mixing in an agate mortar, the resulting mixtures were pre-heated at $900\text{ }^\circ\text{C}$ for 2 h, and then heated at $1300\text{ }^\circ\text{C}$ for 6 h under a 5% $\text{H}_2/95\%\text{ N}_2$ reducing atmosphere. Finally, the samples were cooled to room temperature in the furnace and ground again for the following characterization.

2.2. Characterization

The crystal structure of the samples was identified by X-ray diffraction (XRD) (Bruker D8 Focus diffractometer, in the 2θ range from 20° to 70° with Cu $K\alpha$ radiation ($\lambda = 1.54056\text{ \AA}$) operating at 40 kV and 30 mA). Structural refinement was carried out by the Rietveld method using the FullProf program. Room temperature photoluminescence (PL) and photoluminescence excitation (PLE) spectra were measured using a HITACHI F-7000 spectrometer. Fluorescence microscope PL images (BX53M Instruments; OLYMPUS, Japan) of the powder particles were recorded in dark-field mode upon excitation using a 350 nm UV lamp. The internal quantum efficiencies (QEs) were also measured by an Edinburgh Instruments FLS-920 spectrometer equipped with an Edinburgh Instruments integrating sphere (Edinburgh Instruments, U.K.). The internal QE values were calculated using the quantum yield measurement software. The internal QE defined as the ratio of the number of photons emitted (I_{em}) to the number of photons absorbed (I_{abs}) is expressed as

$$I_{\text{QE}} = \frac{I_{\text{em}}}{I_{\text{abs}}} = \frac{\int L_s}{\int E_{\text{R}} - \int E_{\text{S}}} \quad (1)$$

where L_s is the emission spectrum of the sample, and E_{S} and E_{R} are the spectra of excitation light with and without the sample in the integrating sphere.

The fluorescence decays of Ce^{3+} were measured using an FLS920 fluorimeter (Edinburgh Instruments, Livingston, UK) with a hydrogen flash lamp (nF900; Edinburgh Instruments). The temperature-dependent PL spectra were also recorded on an F-7000 spectrometer with an external heater. A process controller (OMEGA CN76000) equipped with a thermocouple was used to measure temperature and control the heating rate.

A white LED was fabricated by combining a UV-LED chip (365 nm) with a commercial blue phosphor BAM: Eu^{2+} , the as-synthesized BYSF:2% $\text{Ce}^{3+},40\%\text{Tb}^{3+}$ and a commercial red phosphor (Ca,Sr)AlSiN₃: Eu^{2+} . The optical properties of the fabricated w-LEDs were measured using an integrated sphere spectroradiometer system (LHS-1000, Everfine Co., Hangzhou, China). The LED was operated at a bias current of 20 mA and a voltage of 3.4 V. All the measurements were conducted at room temperature unless mentioned otherwise.

3. Results and discussion

3.1. Structural properties

The representative XRD patterns of the as-synthesized samples BYSF:2% Ce^{3+} , BYSF:2% $\text{Ce}^{3+},20\%\text{Tb}^{3+}$ and BYSF:2% $\text{Ce}^{3+},40\%\text{Tb}^{3+}$ are shown in Fig. 1a, and the calculated XRD pattern of BYSF from the Rietveld structural refinement (see below) is also shown for

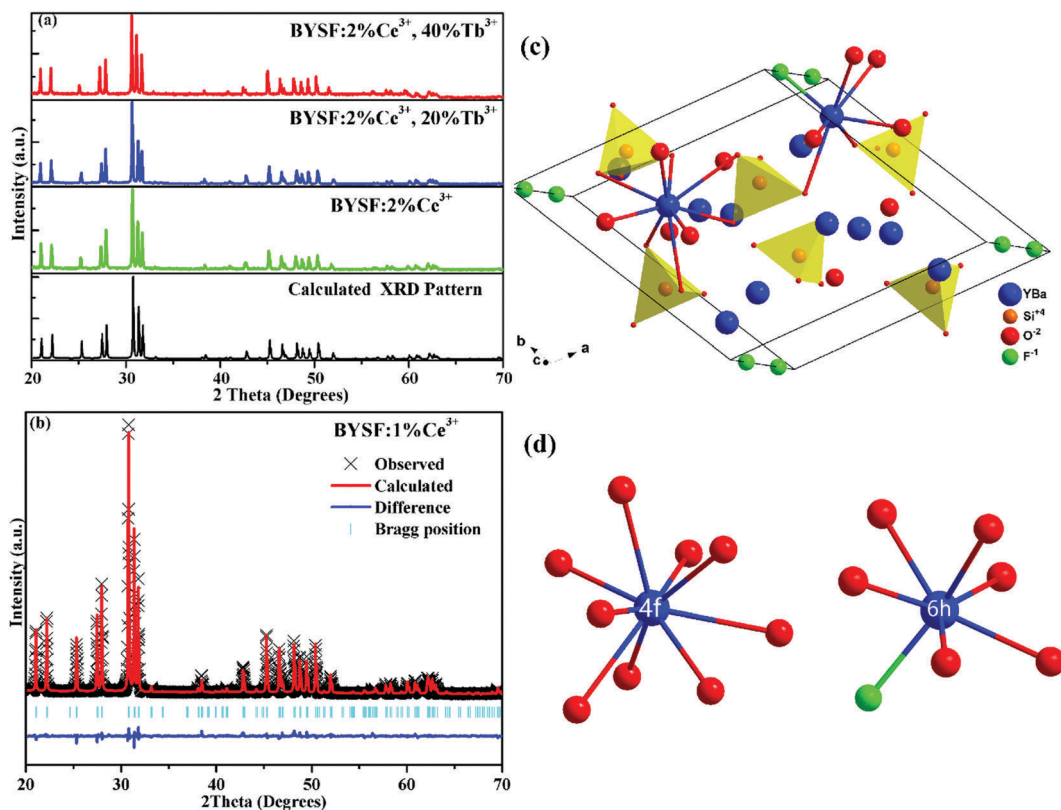


Fig. 1 (a) XRD patterns of BYSF:2%Ce³⁺, BYSF:2%Ce³⁺,20%Tb³⁺ and BYSF:2%Ce³⁺,40%Tb³⁺; (b) Rietveld refinements of XRD data for BYSF:1%Ce³⁺; (c) the crystal structure of BYSF; (d) the coordination environment of the 4f site and the 6h site.

comparison. The XRD patterns of the Tb³⁺ and/or Ce³⁺ doped samples match well with that of BYSF and no impurity phase is detected, indicating the formation of single-phase solid solutions. In addition, with the increase of Tb³⁺ concentration, the diffraction peaks gradually shift to a low diffraction degree, which is expected since the substitution of larger Ce³⁺ ($r = 1.20 \text{ \AA}$ when CN = 9; $r = 1.07 \text{ \AA}$ when CN = 7) and Tb³⁺ ($r = 1.10 \text{ \AA}$ when CN = 9; $r = 0.98 \text{ \AA}$ when CN = 7) for smaller Y³⁺ ($r = 1.08 \text{ \AA}$ when CN = 9; $r = 0.96 \text{ \AA}$ when CN = 7) leads to lattice expansion.³⁸ In order to further investigate the structure of the as-synthesized samples, Rietveld structural refinements for the compositions of BYSF:1%Ce³⁺, x %Tb³⁺ ($x = 0, 66.6, \text{ and } 99$) were performed by using the previously reported crystallographic data of Ba₄La₆(SiO₄)₆F₂ as a starting model.³⁹ The observed, calculated and the different patterns of the XRD refinement of BYSF:1%Ce³⁺ are shown in Fig. 1b. The crystallographic data and refinement parameters of BYSF:1%Ce³⁺, x %Tb³⁺ ($x = 0, 66.6, \text{ and } 99$) are listed in Table 1. All the final weighted R factors (R_{wp}) are acceptable, thus confirming the phase purity of these samples. As illustrated in Fig. 1c, the obtained BYSF crystallizes in the hexagonal space group P6₃/m according to the refinement results and there are two cation sites to occupy for Ba²⁺ and Y³⁺. One is the 4f site (C₃ symmetry) coordinated with nine oxygen atoms and the other is the 6h site (C_s symmetry) coordinated with six O atoms and one F atom. It has been argued that Ba²⁺ only occupies the 4f site since it has very large ionic radii, while the smaller Y³⁺ occupies the 6h site. However, it should be noted that for those relatively large rare earth ions like Ce³⁺ as well as La³⁺, they also have the possibility

to occupy the 4f site. Therefore, when Ce³⁺ is introduced into the BYSF crystal, two emission centres will be formed, which has been confirmed by Yu *et al.* from their different excitation spectra and luminescence decay curves.³⁷

3.2. Photoluminescence properties

As shown in Fig. 2a, the PLE spectrum monitored at 425 nm of Ce³⁺ singly doped BYSF exhibits a broad band ranging from 250 to 400 nm with two distinct excitation band peaks at 295 and 355 nm, which are assigned to the 4f–5d transitions of Ce³⁺. Such a broad excitation band should arise from the superimposition of at least four subbands due to the existence of two kinds of Ce³⁺, and its longer wavelength side matches well with

Table 1 Rietveld refinement, crystallographic and structural parameters of the representative samples BYSF:1%Ce³⁺, x %Tb³⁺ ($x = 0, 66.6, \text{ and } 99$)

Compound	$x = 0$	$x = 66.6$	$x = 99$
Space group	P6 ₃ /m	P6 ₃ /m	P6 ₃ /m
$a = b$ (Å)	9.7408(7)	9.7504(3)	9.7565(0)
c (Å)	7.0298(7)	7.0597(6)	7.0786(0)
$\alpha = \beta$ (deg)	90	90	90
γ (deg)	120	120	120
V (Å ³)	577.662	581.258	583.534
Z	2	2	2
R_p (%)	8.62	11.2	12.7
R_{wp} (%)	9.00	9.72	10.5
R_{exp} (%)	3.44	4.53	5.34
χ^2	6.83	4.6	3.86

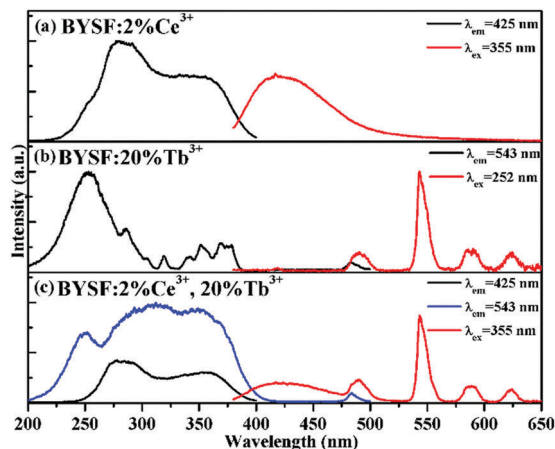


Fig. 2 The PLE and PL spectra of BYSF:2%Ce³⁺ (a), BYSF:20%Tb³⁺ (b) and BYSF:2%Ce³⁺, 20%Tb³⁺ (c).

the emission of an n-UV LED chip. Under 355 nm excitation, the Ce³⁺ doped BYSF shows intense blue emission with an asymmetric emission band peak at 425 nm, resulting from the transitions of Ce³⁺ from the lowest 5d level to the doublet ground levels (²F_{5/2} and ²F_{7/2}) of the 4f configurations. One may notice that most of the emission of Ce³⁺ doped BYSF is shorter than 450 nm in wavelength, which is unfavorable for its application in w-LEDs as a blue phosphor. As for Tb³⁺ singly doped BYSF (Fig. 2(b)), upon UV light (252 nm) excitation, its PL spectrum shows a series of strong emission lines at 490, 543, 585, and 624 nm originating from the ⁵D₄ → ⁷F_J (J = 6, 5, 4, and 3) characteristic transitions of Tb³⁺. The PLE spectrum of the green emission at 543 nm (⁵D₄ → ⁷F₅) contains not only the typical strong excitation band in the range of 200–300 nm that is attributed to the first spin-allowed 4f–5d transitions of Tb³⁺, but also some weak excitation lines in the range of 350–380 nm and at 484 nm due to the 4f–4f forbidden transition lines (350–400 nm) of Tb³⁺. Apparently, Tb³⁺ singly doped BYSF cannot be effectively excited by the n-UV light and thus is useless for w-LEDs. However, the obvious overlap between the emission band of Ce³⁺ and the 4f–4f excitation lines of Tb³⁺ around 484 nm indicates the possibility of energy transfer from Ce³⁺ to Tb³⁺, leading to large color tunability from bluish violet to yellowish green in Ce³⁺ and Tb³⁺ codoped BYSF. It can be seen from Fig. 2(c) that the PLE spectrum for monitoring the Tb³⁺ emission at 543 nm shows the remarkable 5d bands of Ce³⁺ in the range of 300–400 nm, which is similar to that of Ce³⁺ emission at 425 nm. Moreover, under 355 nm excitation, the PL spectrum contains not only the emission band of Ce³⁺ but also the emission lines dominated by the green emission at 543 nm of Tb³⁺. These two features illustrate the occurrence of energy transfer from Ce³⁺ to Tb³⁺ in the Ce³⁺ and Tb³⁺ codoped BYSF. Therefore, codoping Ce³⁺ as a sensitizer for the Tb³⁺ activated phosphor is an effective way to enhance the absorptivity of excitation light in the n-UV region, thereby achieving an efficient green phosphor for w-LEDs based on the n-UV LED.

In order to further study the energy transfer process from Ce³⁺ to Tb³⁺, the emission intensities of Ce³⁺ and Tb³⁺ as a

function of Tb³⁺ concentration were measured. Fig. 3(a) shows the PL spectra of the sample series BYSF:2%Ce³⁺, x%Tb³⁺ with a fixed Ce³⁺ concentration at 2 mol% and various Tb³⁺ concentrations (x = 0–98) under 355 nm excitation. Upon the introduction of Tb³⁺ ions, the emission lines dominated by 543 nm of Tb³⁺ appear accompanied by a decline of the blue emission band of Ce³⁺. As x increases from x = 0 to x = 98, the green emission line at 543 nm due to the ⁵D₄ → ⁷F₅ transition of Tb³⁺ dominates the PL spectrum gradually (see Fig. 3(a)), resulting from the enhanced energy transfer from Ce³⁺ to Tb³⁺. Accordingly, the emission color is tuned from blue to cyan and finally to green, which can be clearly seen from fluorescence microscopy PL images recorded under 350 nm excitation in Fig. 3(c)–(e). As shown in Fig. 3(b), the PL intensity of Tb³⁺ reaches a maximum value at x = 40, beyond which it starts to decrease due to concentration quenching among Tb³⁺ ions. Importantly, as one of the key parameters for practical application in white LEDs, the internal QE of Ce³⁺ and Tb³⁺ codoped BYSF shows no decrease compared to that of Ce³⁺ singly doped BYSF with increasing Tb³⁺ content before concentration quenching occurs (see Table 2), indicating there is no QE loss during the energy transfer process from Ce³⁺ to Tb³⁺. It is noteworthy, however, that in other codoped systems like Ce³⁺–Eu²⁺, Ce³⁺ (Eu²⁺)–Mn²⁺ and Ce³⁺ (Eu²⁺)–Pr³⁺, the QE loss is inevitable since those acceptors usually have low QE values.⁴⁰ Additionally, the internal QE of BYSF:2%Ce³⁺, 40%Tb³⁺ was determined to be as high as 83.12% under 355 nm excitation, which is higher than that of the reported Ce³⁺ and Tb³⁺ codoped phosphors, as listed in Table 2, implying its potential application in white LEDs as a green phosphor.

Based on the Tb³⁺ concentration dependence of the PL intensity of Ce³⁺ shown in Fig. 3, the energy transfer efficiency from Ce³⁺ to Tb³⁺, η_{ET}, can be calculated by:

$$\eta_{ET} = 1 - \frac{I}{I_0} \quad (2)$$

where I₀ and I are the PL intensities of Ce³⁺ in the absence and presence of Tb³⁺, respectively. As listed in Table 3, the calculated energy transfer efficiency becomes larger with increasing Tb³⁺ concentration and reaches 91% at x = 40 where the Tb³⁺ emission is the highest. Considering that there is no QE loss at this point, these results demonstrate that the energy transfer from Ce³⁺ to Tb³⁺ in BYSF is very efficient.

Nonradiative energy transfer from one center to another usually occurs *via* (a) electric multipole–multipole interactions or (b) exchange interactions.^{43,44} As the Ce³⁺ emission corresponds to the allowed electric dipole 5d–4f transition, only the electric dipole–multipole should be considered in the energy transfer from Ce³⁺ to Tb³⁺, excluding the quadrupole–multipole interaction or a higher-order one. The probability of energy transfer from a sensitizer to an activator *via* the electric dipole–dipole interaction is proportional to the oscillator strength of the dipole transition in the activator.⁴⁵ The oscillator strength of the dipole transition from ⁷F₆ to ⁵D₄ in the Tb³⁺ ion is very low (typically 10^{−8}),⁴⁶ even lower than those transitions of Eu³⁺, Sm³⁺ and Dy³⁺ where, experimentally, energy transfer from Ce³⁺ to these ions was hardly observed. Consequently, the electric

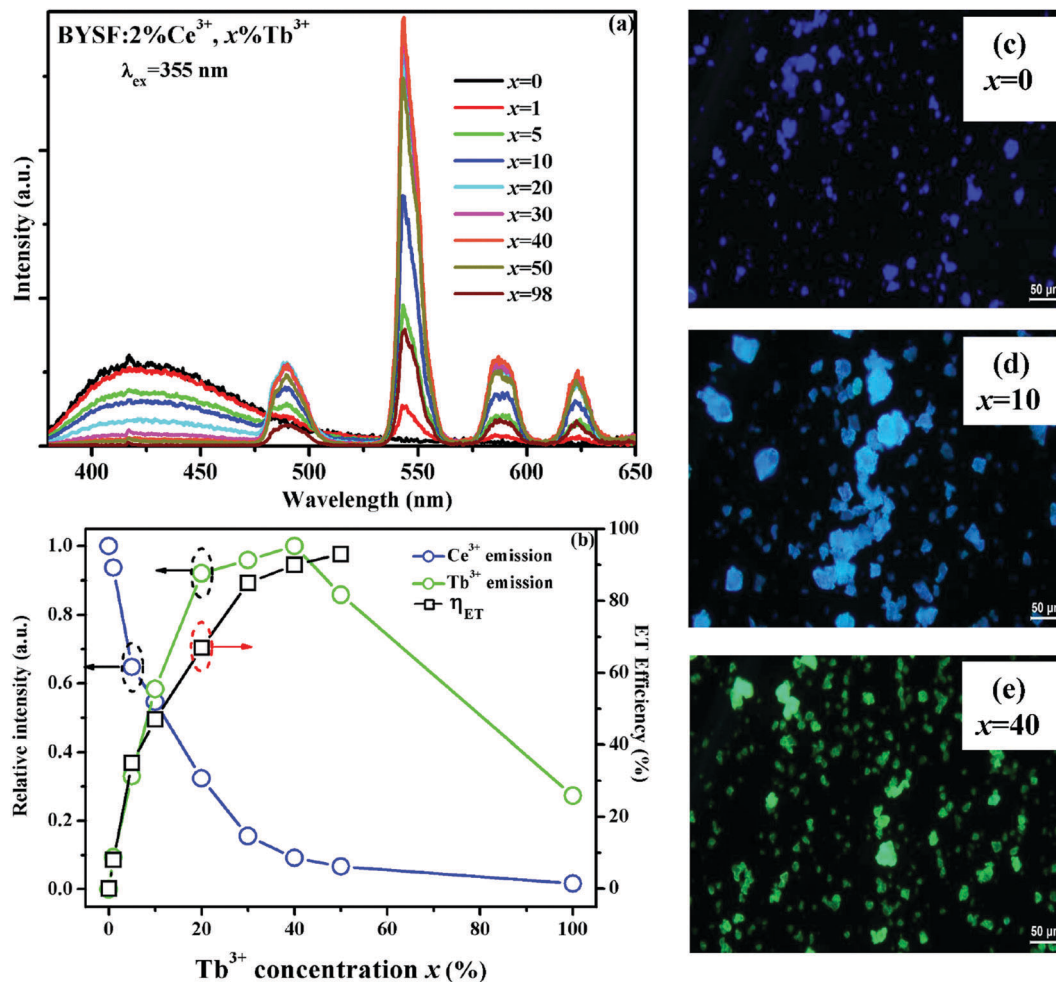


Fig. 3 (a) The PL spectra of the sample series BYSF:2%Ce³⁺, x%B³⁺ ($x = 0-98$) under 355 nm excitation; (b) the emission intensities of Ce³⁺ and Tb³⁺, and the energy transfer efficiency η_{ET} as a function of Tb³⁺ concentration under 355 nm excitation; (c-e) the fluorescence microscopy PL images of BYSF:2%Ce³⁺, x%B³⁺ ($x = 0, 10,$ and 40) under 355 nm excitation.

Table 2 The internal QE of BYSF:2%Ce³⁺, x%B³⁺ ($x = 0, 10, 20,$ and 40) and selected results from the reported references

Samples	QE (%)	Note
BYSF:2%Ce ³⁺	84.05	This work
BYSF:2%Ce ³⁺ , 10%B ³⁺	83.64	This work
BYSF:2%Ce ³⁺ , 20%B ³⁺	83.27	This work
BYSF:2%Ce ³⁺ , 40%B ³⁺	83.12	This work
CaScAlSiO ₆ :0.02Ce ³⁺ , 0.12Tb ³⁺	79.5	Ref. 18
NaBaScSi ₂ O ₇ :0.04Ce ³⁺ , 0.04Tb ³⁺	36	Ref. 34
Sr ₃ CaBa(PO ₄) ₃ Cl:0.05Eu ²⁺ , 0.3Tb ³⁺	72.7	Ref. 35
Ba ₂ Y ₃ B ₅ O ₁₇ :1%Ce ³⁺ , 20%B ³⁺	76	Ref. 36
MgY ₄ Si ₃ O ₁₃ :0.2Ce ³⁺ , 0.4Tb ³⁺	49	Ref. 41
BaY _{1.10} Si ₃ O ₁₀ :0.05Ce ³⁺ , 0.85Tb ³⁺	81.6	Ref. 42
(Ce _{0.67} Tb _{0.33})MgAl ₁₁ O ₁₉	75.3	Ref. 42

Table 3 The calculated energy transfer efficiencies of BYSF:2%Ce³⁺, x%B³⁺ ($x = 0-50$)

x	$\eta_{ET} = 1 - I/I_0$ (%)	$\eta_{ET}' = 1 - \tau/\tau_0$ (%)
0	0	0
1	0.08	0.04
5	0.35	0.12
10	0.47	0.16
20	0.67	0.38
30	0.85	0.50
40	0.90	0.69
50	0.93	0.74

proposed by Blasse, R_c can be estimated geometrically by the following equation:⁴⁷

$$R_c \approx 2 \left[\frac{3V}{4\pi X_c N} \right]^{1/3} \quad (3)$$

where V is the volume of the unit cell, X_c the critical concentration of doped ions, and N the number of total sites to be occupied by the doped ions in the unit cell. In our case, $V = 577.66 \text{ \AA}^3$, $N = 6$, and X_c is the total concentration of the Ce³⁺ and Tb³⁺ ions, *i.e.*, approximately

dipole-dipole interaction can be ruled out as the dominant transfer mechanism. A critical distance, R_c , *i.e.*, the distance at which the probability of energy transfer is equal to that of the radiative transition of the sensitizer, is a classical approach for assigning the main transfer mechanism; for an exchange interaction, R_c is restricted to about 4 Å; however, for a multipolar interaction, this distance can be larger than 10 Å. As

0.36. R_c was therefore calculated to be 7.99 Å, indicating that an exchange interaction may play a negligible role in this situation. Moreover, the admixture of the 4f orbitals of Tb^{3+} and the 2p orbitals of O^{2-} is expected to be small, since the energy necessary for the transfer of one electron from O^{2-} to Tb^{3+} is estimated to be about 64 000 cm^{-1} , which is much higher than that of Eu^{3+} (36 000 cm^{-1}).⁴⁵ Thus, the exchange interaction is very limited.

As Versteegen *et al.* argued, the energy transfer from Ce^{3+} to Tb^{3+} occurs mainly by the electric dipole–quadrupole interaction.^{45,47} According to Dexter's expression and Reisfeld's approximation,^{43,48} the dependence of the PL intensity of a sensitizer on the activator concentration can be used to identify the transfer mechanism, and the energy transfer from Ce^{3+} to Tb^{3+} was determined to be the electric dipole–quadrupole interaction in most of the previous work. However, some of them concluded that the electric dipole–dipole interaction or others were the dominant one.^{49–51} This discrepancy should be ascribed to the fact that the concentration dependence of the PL intensity is a rather insensitive test of mechanism because the ratio of the PL intensities is just approximately equal to that of the luminescence quantum efficiencies;⁵² therefore, Inokuti and Hirayama stated that it is useless to discuss the mechanism of energy transfer only from the slope of concentration dependence,^{44,53} and Birgeneau has also questioned its practicability in identifying the transfer mechanism in ruby.⁵⁴ Besides, as the concentration of Ce^{3+} investigated was fixed at 1 mol% or even higher and the electric dipole–dipole interaction between Ce^{3+} ions is therefore dominant, the excitation energy diffusion among the Ce^{3+} ions followed by the $Ce^{3+} \rightarrow Tb^{3+}$ energy transfer plays an important role in the energy transfer process.^{55,56} Such a diffusion allows the excitation energy to reach farther Tb^{3+} ions, thereby leading to the falsely identified electric dipole–dipole interaction that occurs at a relatively large distance. Although the shortest Tb^{3+} – Tb^{3+} distance in BYSF is only 3.55 Å, a large amount of Tb^{3+} (> 40 mol%) is needed to completely quench the Ce^{3+} emission. Consequently, we believe that the energy transfer from Ce^{3+} to Tb^{3+} mainly takes place by the electric dipole–quadrupole interaction. Accordingly, the probability of energy transfer from Ce^{3+} to Tb^{3+} is proportional to R^{-8} , where R is the distance from Ce^{3+} to Tb^{3+} .⁴⁷ As a result, the $Ce^{3+} \rightarrow Tb^{3+}$ transfer probability for the next-nearest neighbor Tb^{3+} of Ce^{3+} (6.56 Å) is expected to be about two orders of magnitude smaller than that for the nearest neighbor Tb^{3+} of Ce^{3+} (3.55 Å) given that both the Ce^{3+} and Tb^{3+} ions are randomly distributed, which indicates that energy transfer from Ce^{3+} to Tb^{3+} mainly occurs in the nearest Ce^{3+} – Tb^{3+} pairs requiring a high concentration of Tb^{3+} .

To confirm the energy transfer from Ce^{3+} to Tb^{3+} , the decay curves of the Ce^{3+} 5d–4f emission (425 nm) in BYSF:2% Ce^{3+} , x % Tb^{3+} ($x = 0$ –50) under 355 nm excitation were measured. It can be seen from Fig. 4 that the decay curve of Ce^{3+} deviates from the single exponential profile with the introduction of Tb^{3+} , and becomes steeper and steeper with increasing concentration, indicating the occurrence of nonradiative energy transfer from Ce^{3+} to Tb^{3+} . The effective lifetime of Ce^{3+} is defined as:

$$\tau = \frac{\int_0^{\infty} tI(t)dt}{\int_0^{\infty} I(t)dt} \quad (4)$$

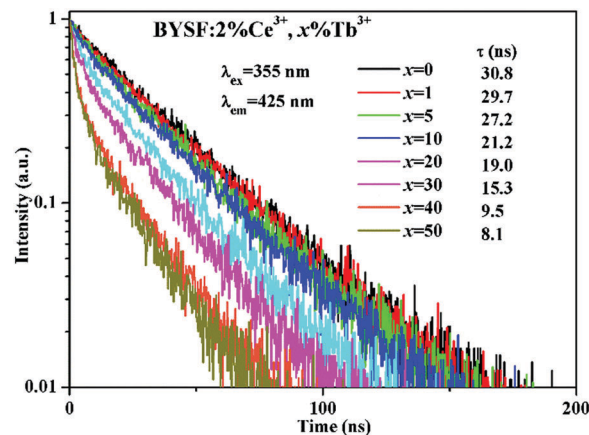


Fig. 4 Fluorescence decay curves of Ce^{3+} in BYSF:2% Ce^{3+} , x % Tb^{3+} ($x = 0$ –50) phosphors (excited at 355 nm and monitored at 425 nm).

where $I(t)$ is the intensity at time t . As shown in Fig. 4, one can find that the effective lifetime decreases monotonically with Tb^{3+} concentration, which strongly demonstrates the energy transfer from Ce^{3+} to Tb^{3+} . The energy transfer efficiency, η_{ET}' , from Ce^{3+} to Tb^{3+} can be calculated by the following equation:

$$\eta_{ET}' = 1 - \frac{\tau}{\tau_0} \quad (5)$$

where τ and τ_0 are the lifetimes of Ce^{3+} in the presence and absence of Tb^{3+} , respectively. The calculated energy transfer efficiencies from Ce^{3+} to Tb^{3+} using eqn (5) are given in Table 3, from which one can find that the transfer efficiency η_{ET}' becomes larger with increasing x and reaches 74% at $x = 50$, indicating an enhanced energy transfer with increasing Tb^{3+} concentration. However, one may notice that the values calculated by eqn (5) are apparently smaller than those calculated by eqn (2). This phenomenon explains that those Ce^{3+} having nearest neighbor Tb^{3+} will decay extremely fast due to the very large energy transfer rate to Tb^{3+} , so that their emission is quenched without luminescence being detected, leading to the absence of the fast decay part in the decay curve of Ce^{3+} and thus smaller reduction of the calculated effective lifetime of Ce^{3+} in Ce^{3+} and Tb^{3+} codoped BYSF.^{36,57} Actually, since the electric dipole–quadrupole interaction is strongly dependent on the interionic distance and the corresponding energy transfer mainly occurs in the nearest ion–ion pairs, the initial part of the decay curve of a sensitizer will be very steep;⁵⁸ therefore, the detected decay curve represents only the slow part of the whole decay process, *i.e.* the decay of those Ce^{3+} without nearest neighbor Tb^{3+} .

3.3. Photoluminescence thermal stability

One of the requirements that phosphors for w-LEDs should fulfil is maintaining their PL intensity at an elevated temperature, typically at 150 °C or even higher for high-power applications. The temperature-dependent PL intensities of the as-prepared BYSF:2% Ce^{3+} , x % Tb^{3+} ($x = 0, 10, 20$, and 40) as well as BYSF:40% Tb^{3+} are given in Fig. 5. The PL intensity of the Ce^{3+} singly doped sample under 330 nm excitation declines rapidly with increasing temperature and drops to only 44% of that at 30 °C when the temperature is raised up to 150 °C, which demonstrates that Ce^{3+} doped BYSF

possesses poor thermal stability. It should be noted that the above result is inconsistent with that of the previous paper³⁷ where Ce³⁺ doped BYSF was reported to have high thermal stability (86% at 150 °C) and the reason is unclear. It is interesting and desirable that the overall PL intensity of the resulting samples decreases more and more slowly with increasing temperature, as Tb³⁺ is increasingly codoped into Ce³⁺ doped BYSF, indicating improved thermal stability by the introduction of Tb³⁺ from 44% in BYSF:2%Ce³⁺ to 78% in BYSF:2%Ce³⁺,40%Tb³⁺ at 150 °C. In the measurement of the above temperature-dependent PL spectra, the excitation light was set at 330 nm so as to eliminate the interference of the absorption of the excitation light by Tb³⁺ itself. One can also find from Fig. 5(c) that the PL intensity of Tb³⁺ singly doped BYSF drops very slowly with the increase of temperature, and still maintains 90% at 150 °C, indicating an excellent thermal stability of Tb³⁺, as expected. We further separated the emission of Tb³⁺ from that of Ce³⁺ in the PL spectra of codoped samples and therefore obtained the temperature-dependent PL intensities originating from Ce³⁺ and Tb³⁺, respectively. As shown in Fig. 5(b) and (c), the thermal stability of Tb³⁺ becomes much better with Tb³⁺ concentration while that of Ce³⁺ gets a little worse. The latter is attributed to smaller bandgaps of the BYSF host and thus enhanced thermal ionization of the excited 5d electron since Y³⁺ is largely replaced by Tb³⁺.⁵⁹ The improved thermal stability of Tb³⁺ is, however, strongly dependent on Tb³⁺

concentration. As proposed in our previous work,³⁶ the thermal quenching of Ce³⁺ emission and nonradiative energy transfer from Ce³⁺ to Tb³⁺ are two competing processes; if the transfer rate is smaller than that of thermal quenching, the thermal stability of Tb³⁺ emission will be almost coincident with that of Ce³⁺ emission; however, if the transfer rate is considerably larger, Tb³⁺ will be independent of that of its sensitizer Ce³⁺ in the thermal stability of emission because the excitation energy of Ce³⁺ has been transferred to Tb³⁺ having much better thermal stability before thermal quenching happens. We have argued that energy transfer from Ce³⁺ to Tb³⁺ mainly occurs in the nearest Ce³⁺-Tb³⁺ pairs *via* the electric dipole-quadrupole interaction. As with a Perrin model,^{36,44,57} Ce³⁺ emission will be completely quenched by fast energy transfer to Tb³⁺ within nearest Ce³⁺-Tb³⁺ pairs, which is supported by the large difference between the energy transfer efficiencies calculated by eqn (2) and by eqn (5), respectively. Consequently, it is not surprising that the improved thermal stability is Tb³⁺ concentration-dependent because with more Tb³⁺, there are more nearest Ce³⁺-Tb³⁺ pairs. Besides, it has been believed that the thermally activated energy back transfer from Tb³⁺ to Ce³⁺ is also possible because the excited electron at the Tb³⁺ ⁵D₄ level has a very long lifetime of several milliseconds.^{31,32,36} Such a back transfer will result in poor thermal stability of Tb³⁺ emission in the Ce³⁺ and Tb³⁺ codoped system. Theoretically, one approach to overcome this problem is to transfer

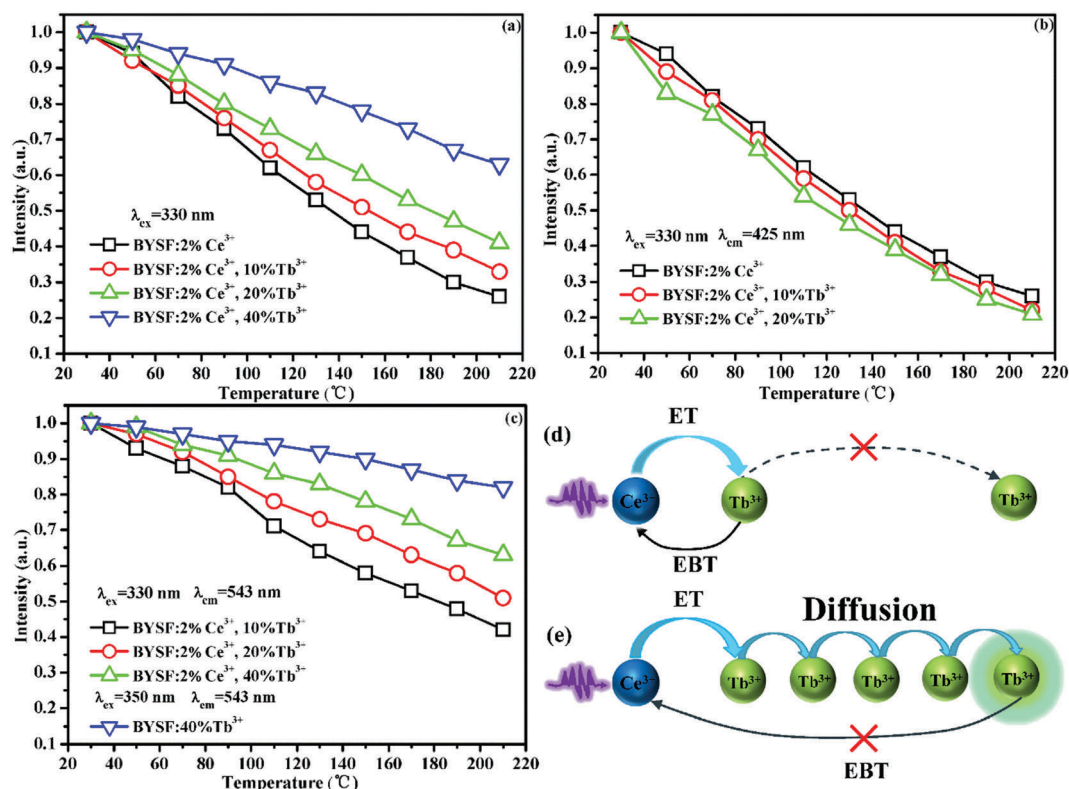


Fig. 5 The temperature-dependent PL intensities of both Ce³⁺ and Tb³⁺ (a), single Ce³⁺ (b), and single Tb³⁺ (c); (d and e) schematic explanation of excitation energy diffusion among Tb³⁺ ions on the thermal stability of the Tb³⁺ emission in the Ce³⁺ and Tb³⁺ codoped system. If the Tb³⁺ concentration is relatively low, thermally excited energy back transfer from Tb³⁺ to Ce³⁺ is possible. If, however, the Tb³⁺ concentration is high enough, fast energy diffusion among the Tb³⁺ ions will compete with such an energy back transfer, thereby preventing its occurrence.

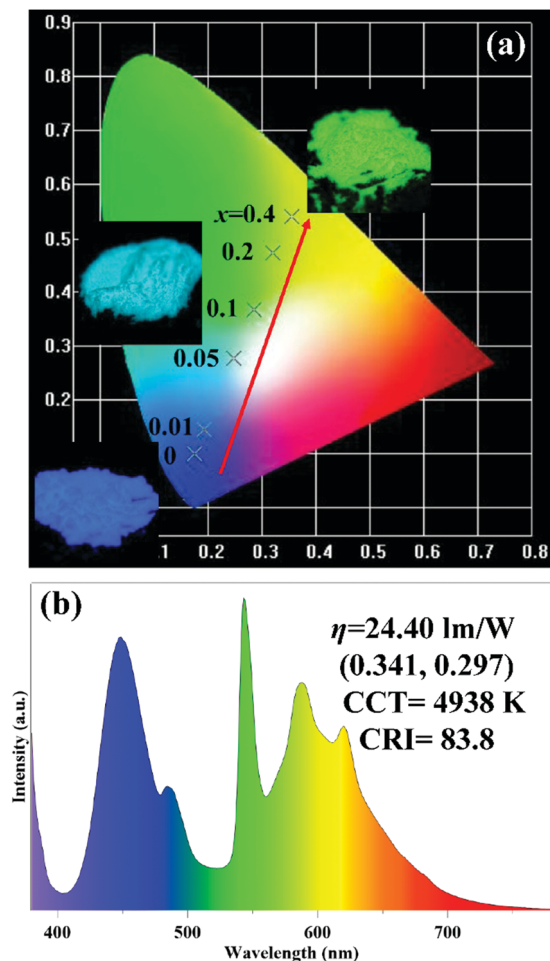


Fig. 6 (a) The CIE chromaticity coordinates of BYSF:2%Ce³⁺,x%Tb³⁺ ($x = 0, 1, 5, 10, 20,$ and 40) under 355 nm excitation and the insets show the digital photos of the selected samples ($x = 0, 10,$ and 40) under 365 nm UV lamp excitation; (b) EL spectrum of a w-LED using a UV-LED chip (365 nm) and BAM:Eu²⁺, BYSF:2%Ce³⁺,40%Tb³⁺ and (Ca,Sr)AlSiN₃:Eu²⁺ phosphors.

the excitation energy of Tb³⁺, the nearest neighbor of Ce³⁺, to a more distant Tb³⁺ as soon as possible by shortening the Tb³⁺-Tb³⁺ distance (as shown in Fig. 5(d) and (e)), which has been used to improve the luminescence efficiency in lanthanide complexes.⁶⁰ From this aspect, increasing the Tb³⁺ concentration is beneficial to the thermal stability of Ce³⁺ and Tb³⁺ codoped phosphors, as can be seen in our case. But it is still not completely clear how these processes compete with each other in determining the luminescence properties, which needs further research.

3.4. Electroluminescence spectrum of the fabricated w-LED device

Fig. 6 shows the Commission International de l'Éclairage (CIE) chromaticity coordinates of the samples BYSF:2%Ce³⁺,x%Tb³⁺ ($x = 0, 1, 5, 10, 20,$ and 40) under 355 nm excitation. The emission color can be tuned from bluish violet (0.175 and 0.099) to cyan (0.286 and 0.368) and finally to yellowish green (0.354, 0.539) with increasing Tb³⁺ concentration, which is visually reflected by the inserted digital photographs in Fig. 6(a) of the

selected samples upon excitation using a 365 nm UV lamp. It is confirmed that large color tunability achieved *via* codoping Tb³⁺ into BYSF and the as-synthesized BYSF:2%Ce³⁺,40%Tb³⁺ provides the potential for novel green phosphors for w-LEDs based on n-UV LEDs. To demonstrate the potential application of the as-synthesized BYSF:2%Ce³⁺,40%Tb³⁺, a prototype of w-LEDs was fabricated by combining a 365 nm UV LED chip with a mixture of commercial blue phosphor BAM:Eu²⁺, the as-synthesized BYSF:2%Ce³⁺,40%Tb³⁺ and a commercial red phosphor (Ca,Sr)AlSiN₃:Eu²⁺. The electroluminescence (EL) spectrum of the as-fabricated w-LED is shown in Fig. 6(b), where the weight ratio of the three phosphors is $5 : 20 : 3$. The corresponding CRI, CCT, luminous efficiency (η), and CIE chromaticity coordinates were determined to be $83.8, 4938$ K, 24.40 lm W⁻¹ and (0.341, 0.297), respectively. The value of CRI is higher than that of the traditional w-LED product made by combining the yellow phosphor YAG:Ce³⁺ with the blue LED chip ($R_a \approx 75$). The w-LED packaging results indicate that the as-synthesized BYSF:2%Ce³⁺,40%Tb³⁺ is a potential candidate as a green phosphor for w-LEDs based on n-UV LEDs.

4. Conclusions

In summary, BYSF:2%Ce³⁺,x%Tb³⁺ phosphors with tunable emission color were successfully prepared by the high-temperature solid-state reaction. The emission color can be tuned from bluish violet to yellowish green with increasing Tb³⁺ concentration, resulting from the enhanced energy transfer from Ce³⁺ to Tb³⁺. The energy transfer efficiency was calculated to be as high as 91% before concentration quenching among Tb³⁺ ions occurs, and thus a novel efficient green phosphor was developed when $x = 40$, whose internal QE was determined to be 83.12%, indicating no QE loss during the energy transfer process. This has been ascribed to the fast energy transfer within the nearest Ce³⁺-Tb³⁺ pairs *via* the electric dipole-quadrupole interaction. Moreover, thermal stability is improved considerably by increasing the Tb³⁺ concentration, which was well explained by considering not only the fast energy transfer from Ce³⁺ to Tb³⁺ but also the energy diffusion among Tb³⁺ ions. In addition, the w-LED lamp fabricated with an n-UV chip, a blue phosphor BAM:Eu²⁺, a red phosphor (Ca,Sr)AlSiN₃:Eu²⁺ and a green phosphor BYSF:2%Ce³⁺,40%Tb³⁺ produced white light with CRI = 83.8 and CCT = 4938 K. Our results indicate that BYSF:2%Ce³⁺,40%Tb³⁺ has great potential to serve as a green phosphor for w-LEDs based on n-UV LEDs, and fast energy transfer to Tb³⁺ may provide an alternative way of improving the thermal stability of phosphors.

Conflicts of interest

There are no conflicts to declare.

Acknowledgements

This work was partially supported by the National Key R&D Program of China (Grant No. 2016YFB0701003 and 2016YFB0400605), the National Natural Science Foundation of

China (Grant No. 61275055, 11274007, 51402284 and 11604330), the Natural Science Foundation of Jilin Province (Grant No. 20140101169JC, 20150520022JH and 20160520171JH), and the Prior Sci-tech Program of Innovation and Entrepreneurship for Overseas Chinese Talents of Jilin Province.

References

- P. Pust, P. J. Schmidt and W. Schnick, *Nat. Mater.*, 2015, **14**, 454–458.
- S.-H. Lim, Y.-H. Ko, C. Rodriguez, S.-H. Gong and Y.-H. Cho, *Light: Sci. Appl.*, 2016, **5**, e16030.
- J. Cho, J. H. Park and J. K. Kim, *Laser Photonics Rev.*, 2017, **11**, 1600147.
- I. E. Titkov, A. Yadav, S. Y. Karpov, A. V. Sakharov and A. F. Tsatsulnikov, *Laser Photonics Rev.*, 2016, **10**, 1031–1038.
- C. C. Lin, A. Meijerink and R. S. Liu, *J. Phys. Chem. Lett.*, 2016, **7**, 495–503.
- M. H. Fang, C. Ni, X. Zhang, Y. T. Tsai, S. Mahlik, A. Lazarowska, M. Grinberg, H. S. Sheu, J. F. Lee, B. M. Cheng and R. S. Liu, *ACS Appl. Mater. Interfaces*, 2016, **8**, 30677–30682.
- J. McKittrick, M. E. Hannah, A. Piquette, J. K. Han, J. I. Choi, M. Anc, M. Galvez, H. Lugauer, J. B. Talbot and K. C. Mishra, *ECS J. Solid State Sci. Technol.*, 2013, **2**, R3119–R3131.
- T. Nishida, T. Ban and N. Kobayashi, *Appl. Phys. Lett.*, 2003, **82**, 3817–3819.
- P. Dorenbos, *J. Lumin.*, 2000, **91**, 155–176.
- P. Dorenbos, *Phys. Rev. B: Condens. Matter Mater. Phys.*, 2001, **64**, 125117.
- G. Li, Y. Tian, Y. Zhao and J. Lin, *Chem. Soc. Rev.*, 2015, **44**, 8688–8713.
- J. Zhang, B. Xie, X. Yu, X. Luo, T. Zhang, S. Liu, S. Liu, Z. Yu, L. Liu and X. Jin, *J. Appl. Phys.*, 2017, **122**, 043103.
- Z. Xia and Q. Liu, *Prog. Mater. Sci.*, 2016, **84**, 59–117.
- P.-P. Dai, C. Li, X.-T. Zhang, J. Xu, X. Chen, X.-L. Wang, Y. Jia, X. Wang and Y.-C. Liu, *Light: Sci. Appl.*, 2016, **5**, e16024.
- M. Shang, C. Li and J. Lin, *Chem. Soc. Rev.*, 2014, **43**, 1372–1386.
- X. Liu and J. Qiu, *Chem. Soc. Rev.*, 2015, **44**, 8714–8746.
- K. Song, J. Zhang, Y. Liu, C. Zhang, J. Jiang, H. Jiang and H. B. Qin, *J. Phys. Chem. C*, 2015, **119**, 24558–24563.
- W. Lu, N. Guo, Y. Jia, Q. Zhao, W. Lv, M. Jiao, B. Shao and H. You, *Inorg. Chem.*, 2013, **52**, 3007–3012.
- H. S. Jang, W. B. Im, D. C. Lee, D. Y. Jeon and S. S. Kim, *J. Lumin.*, 2007, **126**, 371–377.
- J. Qiao, J. Zhang, X. Zhang, Z. Hao, Y. Liu and Y. Luo, *Dalton Trans.*, 2014, **43**, 4146–4150.
- V. Sivakumar and U. V. Varadaraju, *J. Electrochem. Soc.*, 2009, **156**, J179–J184.
- W. Y. Huang, F. Yoshimura, K. Ueda, Y. Shimomura, H. S. Sheu, T. S. Chan, C. Y. Chiang, W. Zhou and R. S. Liu, *Chem. Mater.*, 2014, **26**, 2075–2085.
- L. Wang, X. Zhang, Z. Hao, Y. Luo, X. J. Wang and J. Zhang, *Opt. Express*, 2010, **18**, 25177–25182.
- L. Wang, R.-J. Xie, Y. Li, X. Wang, C.-G. Ma, D. Luo, T. Takeda, Y.-T. Tsai, R.-S. Liu and N. Hirotsaki, *Light: Sci. Appl.*, 2016, **5**, e16155.
- Y. H. Kim, P. Arunkumar, B. Y. Kim, S. Unithrattil, E. Kim, S. H. Moon, J. Y. Hyun, K. H. Kim, D. Lee, J.-S. Lee and W. B. Im, *Nat. Mater.*, 2017, **16**, 543–550.
- P. F. Smet and J. J. Joos, *Nat. Mater.*, 2017, **16**, 500–501.
- D. Wen, J. Shi, M. Wu and Q. Su, *ACS Appl. Mater. Interfaces*, 2014, **6**, 10792–10801.
- J. Zhou and Z. Xia, *J. Mater. Chem. C*, 2015, **3**, 7552–7560.
- Y. Cui, B. Li, H. He, W. Zhou, B. Chen and G. Qian, *Acc. Chem. Res.*, 2016, **49**, 483–493.
- Z. Dou, J. Yu, Y. Cui, Y. Yang, Z. Wang, D. Yang and G. Qian, *J. Am. Chem. Soc.*, 2014, **136**, 5527–5530.
- W. Xiao, D. Wu, L. Zhang, X. Zhang, Z. Hao, G. H. Pan, H. Zhao, L. Zhang and J. Zhang, *J. Phys. Chem. C*, 2017, **121**, 2998–3006.
- C. C. Lin, W.-T. Chen, C.-I. Chu, K.-W. Huang, C.-W. Yeh, B.-M. Cheng and R.-S. Liu, *Light: Sci. Appl.*, 2016, **5**, e16066.
- Z. L. Wang, Z. W. Quan, P. Y. Jia, C. K. Lin, Y. Luo, Y. Chen, J. Fang, W. Zhou, C. J. O'Connor and J. Lin, *Chem. Mater.*, 2006, **18**, 2030–2037.
- G. Li, Y. Wang, W. Zeng, W. Chen, S. Han, H. Guo and Y. Li, *J. Mater. Chem. C*, 2016, **4**, 3304–3312.
- X. Chen, P. Dai, X. Zhang, C. Li, S. Lu, X. Wang, Y. Jia and Y. Liu, *Inorg. Chem.*, 2014, **53**, 3441–3448.
- Y. Xiao, Z. Hao, L. Zhang, W. Xiao, D. Wu, X. Zhang, G. H. Pan, Y. Luo and J. Zhang, *Inorg. Chem.*, 2017, **56**, 4538–4544.
- R. Yu, H. Li, H. Ma, C. Wang and H. Wang, *J. Am. Ceram. Soc.*, 2014, **97**, 1151–1156.
- R. D. Shannon, *Acta Crystallogr., Sect. A: Cryst. Phys., Diffr., Theor. Gen. Crystallogr.*, 1976, **32**, 751–767.
- Q. Guo, L. Liao and Z. Xia, *J. Lumin.*, 2014, **145**, 65–70.
- J. Wang, H. Lin, Q. Huang, G. Xiao, J. Xu, B. Wang, T. Hu and Y. Wang, *J. Mater. Chem. C*, 2017, **5**, 1789–1797.
- H. Y. Chung, C. H. Lu and C. H. Hsu, *J. Am. Ceram. Soc.*, 2010, **93**, 1838–1841.
- Z. Xia, Y. Liang, D. Yu, M. Zhang, W. Huang, M. Tong, J. Wu and J. Zhao, *Opt. Laser Technol.*, 2014, **56**, 387–392.
- D. L. Dexter, *J. Chem. Phys.*, 1953, **21**, 836–850.
- M. Inokuti and F. J. Hirayama, *Chem. Phys.*, 1965, **43**, 1978–1989.
- J. M. P. J. Versteegen, J. L. Sommerdijk and J. G. Verriet, *J. Lumin.*, 1973, **6**, 425–431.
- W. T. Carnall, P. R. Fields and K. Rajnak, *J. Chem. Phys.*, 1968, **49**, 4412–4423.
- J. L. Sommerdijk and J. M. P. J. Versteegen, *J. Lumin.*, 1974, **9**, 415–419.
- R. Reisfeld, E. Greenberg, R. Velapoldi and B. Barnett, *J. Chem. Phys.*, 1972, **56**, 1698–1705.
- R. Reisfeld and J. Hormadaly, *J. Solid State Chem.*, 1975, **13**, 283–287.
- Z. Xia and R.-S. Liu, *J. Phys. Chem. C*, 2012, **116**, 15604–15609.

- 51 Q. Guo, Q. Wang, L. Jiang, L. Liao, H. Liu and L. Mei, *Phys. Chem. Chem. Phys.*, 2016, **18**, 15545–15554.
- 52 D. J. Robbins, B. Cockayne, B. Lent and J. L. Glasper, *Solid State Commun.*, 1976, **20**, 673–676.
- 53 E. Nakazawa and S. Shionoya, *J. Phys. Soc. Jpn.*, 1970, **28**, 1260–1265.
- 54 R. J. Birgeneau, *J. Chem. Phys.*, 1969, **50**, 4282–4287.
- 55 J. C. Bourcet and F. K. Fong, *J. Chem. Phys.*, 1974, **60**, 34–39.
- 56 R. Sato, S. Takeshita, T. Isobe, T. Sawayama and S. Niikura, *ECS J. Solid State Sci. Technol.*, 2012, **1**, R163–R168.
- 57 L. Feng, Z. Hao, X. Zhang, L. Zhang, G. Pan, Y. Luo, L. Zhang, H. Zhao and J. Zhang, *Dalton Trans.*, 2016, **45**, 1539–1545.
- 58 L. G. Van Uitert, *J. Electrochem. Soc.*, 1967, **114**, 1048–1053.
- 59 J. Ueda, P. Dorenbos, A. J. Bos, A. Meijerink and S. Tanabe, *J. Phys. Chem. C*, 2015, **119**, 25003–25008.
- 60 S. Omagari, T. Nakanishi, Y. Kitagawa, T. Seki, K. Fushimi, H. Ito, A. Meijerink and Y. Hasegawa, *Sci. Rep.*, 2016, **6**, 37008.